ELSEVIER

NeuroImage

www.elsevier.com/locate/ynimg
NeuroImage 29 (2006) 1092 – 1105

White matter fiber tracts of the human brain: Three-dimensional mapping at microscopic resolution, topography and intersubject variability

Uli Bürgel,[a,d] Katrin Amunts,[b,c] Lars Hoemke,[c] Hartmut Mohlberg,[c] Joachim M. Gilsbach,[a] and Karl Zilles[c,d,*]

[a]*Department of Neurosurgery, RWTH Aachen University, D-52074 Aachen, Germany*
[b]*Department of Psychiatry and Psychotherapy, RWTH Aachen University, D-52074 Aachen, Germany*
[c]*Institute of Medicine, Research Center Jülich, and Brain Imaging Center West (BICW), D-52425 Jülich, Germany*
[d]*C. and O. Vogt Institute for Brain Research, University of Düsseldorf, D-40001 Düsseldorf, Germany*

Received 19 May 2005; revised 9 August 2005; accepted 25 August 2005
Available online 19 October 2005

The position and extent of individual fiber tracts within the white matter of human brains can be identified in vivo using diffusion tensor imaging (DTI) and fiber tracking methods. Previous to this study, however, the lack of three-dimensional (3-D) probability maps precluded comparing the anatomical precision of MRI studies with microscopically defined fiber tracts in human postmortem brains. The present study provides 3-D registered maps of the topography, course and intersubject variability of major fiber tracts, which were identified at microscopic resolution. The analyzed tracts include the corticospinal tract, optic and acoustic radiations, fornix, cingulum, corpus callosum, superior longitudinal, superior and inferior occipito-frontal and uncinate fascicles; sources and targets of fiber tracts include the lateral and medial geniculate nuclei and mamillary bodies. Tracts and nuclei were identified in serial myelin-stained histological sections of ten postmortem brains. The sections were 3-D reconstructed and registered to a standardized stereotaxic space of an in vivo MR reference brain by means of linear and non-linear, elastic transformations. The individual fiber tracts and nuclei were superimposed in the reference space, and probability maps were generated as a quantitative measure of intersubject variability for each voxel of the stereotaxic space. This study presents the first stereotaxic atlas of the course, location and extent of fiber tracts and related nuclei based on microscopically defined localization and topographic data taken at multiple levels on each of the three orthogonal planes. The maps are useful for evaluating and identifying fiber bundles in DTI, for localizing subcortical lesions visible in anatomical MR images and for studying neuronal connectivity.

Introduction

The rapid development of MR imaging techniques and, in particular, diffusion tensor MRI (DT-MRI) has renewed interest in precise fiber tract anatomy. Previously, microstructural information on the course of major fiber tracts was obtained in immature brains by distinguishing early myelinating fiber tracts from the still non-stained, later myelinating ones (Flechsig, 1920; Yakovlev and Lecours, 1967). Such studies have contributed important information on the topography of fiber tracts and their maturation during ontogeny. They do not, however, provide stereotaxic topographic information about the course and extent of fiber tracts in the (adult) human brain nor do they address intersubject variability and interhemispheric asymmetry, both of which are important aspects of brain anatomy (Zilles et al., 1996, 1997). Tracing studies, which are frequently performed in experimental animals, are either impossible or have restricted application in the human brain. Tracing studies in adult human brains have used, for example, degenerated axons in pathologically altered brains (e.g., Clarke and Miklossy, 1990; Mufson et al., 1990; Miklossy and van der Loos, 1991; Clarke, 1994; Di Virgilio and Clarke, 1997; Wiesendanger et al., 2004) or polarized light microscopy (Axer and Keyserlingk, 2000).

The development of DTI has opened new opportunities for analyzing white matter in the living human brain (e.g., Le Bihan et al., 1986; Turner et al., 1990; Basser and Pierpaoli, 1994; Piearpoli et al., 1996; Iwasawa et al., 1997; Makris et al., 1997; Clark et al., 1999; Conturo et al., 1999; Virta et al., 1999; Werring et al., 1999; Basser et al., 2000; Barker, 2001; Coenen et al., 2001; Krings et al., 2001; Stieltjes et al., 2001; Mori and van Zijl, 2002; Hagemann et al., 2003; Büchel et al., 2004; Schoth and Krings, 2005; Wakana et al., 2004, 2005). The method is based on the fact that measured diffusivity depends on the orientation of the principal axes of fiber tracts (for a review, see, e.g., Basser and

* Corresponding author. Institute of Medicine, Research Center Juelich, and Brain Imaging Center West (BICW), 52425 Juelich, Germany. Fax: +49 2461 61 2990.
E-mail address: k.zilles@fz-juelich.de (K. Zilles).
Available online on ScienceDirect (www.sciencedirect.com).

1053-8119/$ - see front matter © 2005 Elsevier Inc. All rights reserved.
doi:10.1016/j.neuroimage.2005.08.040

Jones, 2002). Fiber tract trajectories are generated from a fluid velocity field. Several fiber tracts of the white matter, the brain stem, the spinal cord as well as single nerves (e.g., optic nerve) have been traced this way, and these studies represent tremendous progress for analyzing connectivity in the adult human brain (Ramnani et al., 2004). Connectivity maps in the macaque brain, obtained using DTI and fast marching tractography (FMT), are consistent with known anatomy (Parker et al., 2002). DT-MRI has been applied successfully to neurological and psychiatric studies to demonstrate and analyze alterations of the white matter in different diseases, such as multiple sclerosis and schizophrenia (Iwasawa et al., 1997; Barker, 2001; Foong et al., 2002; Ardekani et al., 2003, Kubicki et al., 2005). There are, however, limitations of the method (Koch et al., 2002) if discrete, coarsely sampled, noisy, voxel-averaged direction field data are used on incoherently organized nerve pathways (Basser and Jones, 2002) or if fibers merge, branch or cross each other (Le Bihan et al., 2001). DT-MRIs are not capable, in a strict sense, of investigating anatomical connectivity.

Using a modified myelin staining technique, fiber tracts have been mapped in histological sections of ten adult human brains at microscopic resolution, and probabilistic, three-dimensional maps of the optic radiation (Bürgel et al., 1999), the corticospinal tract (Rademacher et al., 2001) and the auditory system (Rademacher et al., 2002) have been published. The aim of the present study was to extend and supplement these studies by mapping ten fiber tracts; corticospinal tract, optic radiation, acoustic radiation, fornix, cingulum, corpus callosum, superior longitudinal fascicle, superior and inferior occipito-frontal fascicles, uncinate fascicle and three associated nuclei; lateral and medial geniculate bodies; and mamillary body. Individual maps were registered to the T_1-weighted single subject brain of the Montreal Neurological Institute ('MNI reference brain'; Evans et al., 1993; Collins et al., 1994; Holmes et al., 1998), generating probabilistic maps. The spatial topography of the structures, their relationships with each other, with surrounding macroscopic landmarks and subcortical nuclei, and their intersubject variability were analyzed via the probabilistic maps.

Materials and methods

Ten human brains (Table 1) without any history of neuropathological or psychiatric diseases in their clinical records or neuropathological alterations in the histological sections were analyzed. Brains were obtained from the body donor program of the Anatomical Institute of the University of Duesseldorf. Handedness of body donors was unknown. High-resolution MR imaging of the brains was performed after fixation and prior to histological embedding and further processing (Roland and Zilles, 1994; Zilles et al., 1995; Amunts et al., 2000; Geyer et al., 1996) with a Siemens 1.5 T scanner (Erlangen, Germany) and a T_1-weighted FLASH sequence (flip angle = 40°; repetition time (TR) = 40 ms; echo time (TE) = 5 ms for each image). The complete brains were fixed in formalin or Bodian solution (a mixture of formalin, glacial acetic acid and ethanol), embedded in paraffin and serially sectioned in the coronal plane at 20 μm. Depending on the size of the brain, a series of 4000 to 7500 sections per brain was obtained. Each 60th section of the complete series (distance between sections: 1.2 mm) was stained with a modified Heidenhain–Woelcke technique for myelin (Bürgel et al., 1997; Figs. 1+2). Neighboring sections were stained for cell bodies (Merker, 1983).

Table 1
Postmortem brains

Case	Age (years)	Gender	Cause of death	Postmortem delay (hours)	Brain weight before fixation (g)
382/81	59	F	Cardio-respiratory insufficiency	24	1142
544/91	79	F	Carcinoma of the bladder	24	1350
56/94	72	F	Renal failure	12	1216
2/95	85	F	Mesenteric artery infarction	14	1046
68/95	79	F	Cardio-respiratory insufficiency	16	1110
207/84	75	M	Toxic glomerulonephritis	24	1349
146/86	37	M	Right heart failure	24	1437
281/93	68	M	Vascular disease	16	1360
16/96	54	M	Myocardial infarct	8	1757
2431	39	M	Drowning	10	1247

Traditional myelin stains can rarely distinguish individual tracts within the densely packed fibers of the adult human white matter. The modification of the Heidenhain–Woelcke stain increases lithium ions, which destain the tissue by inactivating the chromatogen complexes in the thinnest myelin sheaths, thus decreasing the overall background staining and producing a graded reduction in myelin staining on fiber tracts. The reduction appears proportional to the degree of myelination of the tracts. The result enhances the contrast between fiber tracts, enabling us to distinguish different pathways according to their degrees of myelination. In summary, the protocol differentially stains myelinated connections in the adult human brain in a manner resembling the differential staining of fiber tracts during myelination of early postnatal brains.

The myelin-stained sections were digitized via a CCD camera (8 bit gray resolution; depth of field and tissue thickness of 20 μm; final resolution of 0.9 × 0.9 × 1.2 mm per voxel), and 3-D reconstruction followed (Schormann and Zilles, 1998). Deformation of the images of the histological sections that inevitably arise during histological processing (from vagaries of dehydration, embedding, cutting and mounting on glass slides) is corrected using both the MR images of the complete brain prior to embedding and the digitized histological sections. The 3-D reconstructed histological volumes of the ten brains were warped to the single-subject MNI reference brain (Evans et al., 1993; Collins et al., 1994; Holmes et al., 1998; Mohlberg et al., 2003). To align the data with the "anatomical MNI space," they were shifted by 4 mm and 5 mm in the coronal and axial planes, respectively (Amunts and Zilles, in press). The shift placed the brain data sets along the line connecting the anterior and posterior commissures in the midsagittal plane (the AC–PC line), where the orientation and origin correspond to the system proposed by Talairach and Tournoux (1988). Warping was performed using histogram correction, linear, affine and non-linear, elastic transformations (Schormann and Zilles, 1998; Amunts et al., 2004). The elastic image registration is based on the Navier–Lamé equations, which are solved using a multigrid method for the inner iteration with a multiscale approach (Henn et al., 1997; Hömke, 2005).

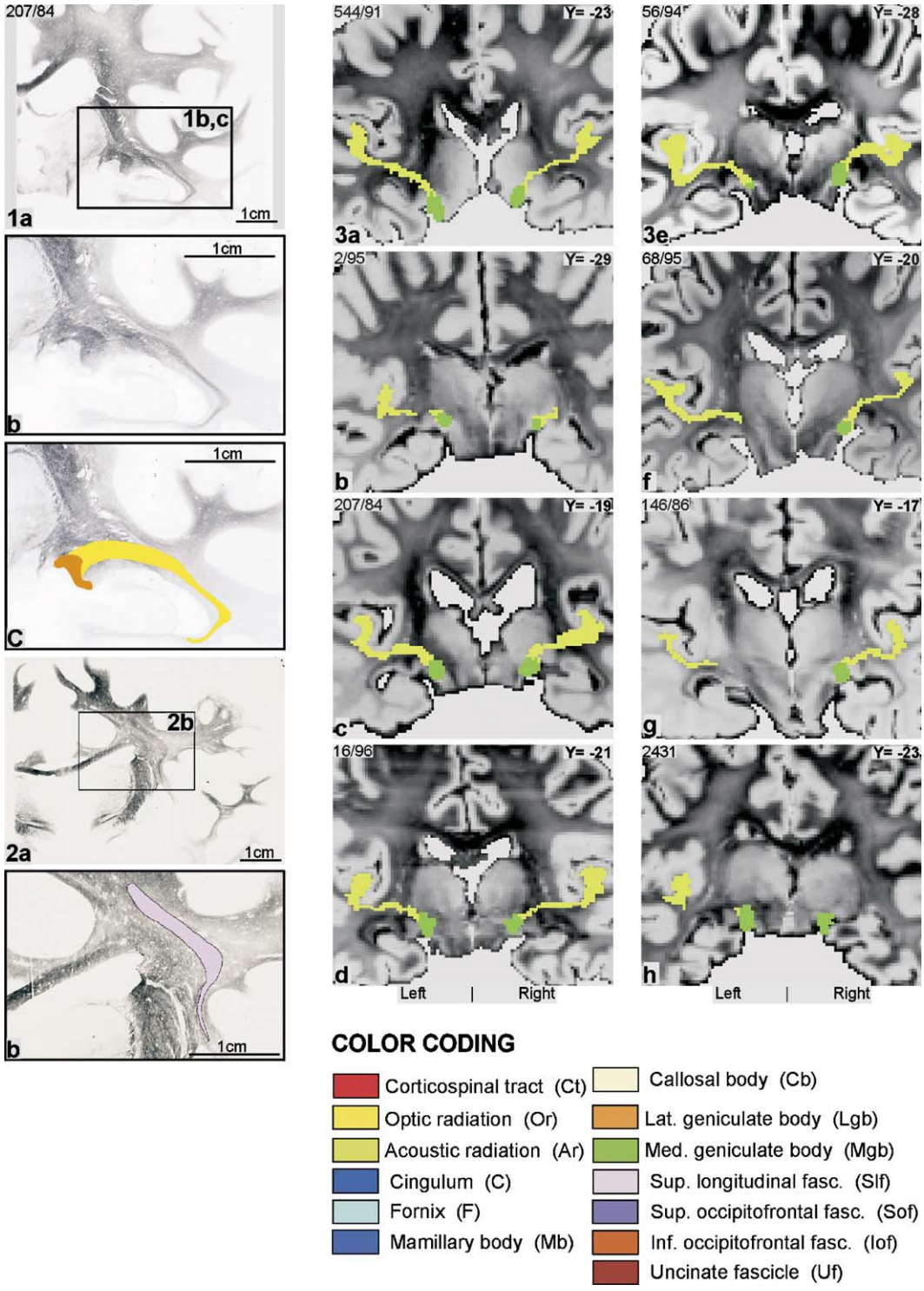

Fig. 1. Histological coronal sections of the right hemisphere of brain 207/84. (a) Myelin staining with a modified Heidenhain–Woelcke stain (Bürgel et al., 1997). (b) The temporal lobe and isthmus in higher magnification of panel a. (c) The same section as in panel b. The optic radiation (yellow) and the lateral geniculate body (orange) have been marked.

Fig. 2. Histological coronal sections of the right hemisphere of brain 2431. (a) Myelin staining with a modified Heidenhain–Woelcke stain (Bürgel et al., 1997). (b) A higher magnification of panel a which highlights the region around the superior longitudinal fascicle (marked in pink) and shows that even the weak myelinated association tracts can be clearly identified from surrounding tissue.

Fig. 3. Coronal sections of eight individual brains with marked acoustic radiation (light green) and medial geniculate bodies (dark green). Orientation in anatomical MNI space (according to the AC–PC plane). Coronal sections at the level of the medial geniculate body, which projects to the Heschl's gyrus via the acoustic radiation. The presence and the shape of the acoustic radiation and the medial geniculate body vary considerably: for example, whereas the acoustic radiation of brain 544/91 runs directly to the Heschl's gyrus, the acoustic radiation of brain 56/94 reaches this gyrus only after a turn down.

The following fiber tracts and subcortical nuclei were microscopically identified (Table 2).

- The corticospinal tract originating from Brodmann's area 4 (Brodmann, 1909), including subareas 4a and 4p (Geyer et al., 1996),
- The optic radiation and the lateral geniculate body (Bürgel et al., 1999),
- The acoustic radiation and the medial geniculate body,
- The fornix and the mamillary body,
- The corpus callosum and
- Long-association fiber tracts including the superior longitudinal fascicle, the superior and inferior occipito-frontal fascicles and the uncinate fascicle.

Fiber tracts and nuclei were identified in both hemispheres of each brain (Figs. 1 and 2) using the descriptions of Kretschmann and Weinrich (1996) and Nieuwenhuys et al. (1988). Both the heavily stained projection fiber tracts and the less intensely stained long-association tracts are differentiated from the background and can, therefore, be precisely identified. This technique also enabled us to map critical regions where fibers cross each other, become microscopically thin, merge or when fibers are densely packed as in the temporal isthmus. Additionally, we used origin and/or target structures, such as the lateral geniculate body and the striate area, to define tracts, like the optic radiation.

Mapping was performed in coronal sections. This cutting plane favors the delineation of those fiber tracts which run in medio-lateral and dorso-ventral directions. It makes it more difficult to follow fibers that go rostro-caudally and which do not appear in the coronal sections as elongated fiber bundles. From this, we may assume that long-association fiber tracts connecting the occipital and frontal lobes are probably underestimated, whereas the corticospinal tract has been defined more completely. We do not, however, expect to overestimate the extent of fiber tracts.

By analyzing the histological texture of the white matter at high magnification (up to 400×), we were able to use differences in the contours of sectioned fibers (fibers running vertically to the plane of sectioning appear as ring-shaped structures at higher magnification, whereas obliquely or parallel running fibers appear as shorter or longer dark lines), in tract orientation (circular contours are observed in vertical tracts, whereas elongated contours are those oblique to the plane of sectioning) and in staining intensity to delineate distinct pathways within a single section and through a series of sections. Thus, we could follow myelinated fibers throughout their entire course. The start and target structures of the acoustic radiation (medial geniculate body and Heschl's gyrus) were identified using immediately adjacent sections, which were stained for cell bodies. The well-known start and/or endpoints of the corticospinal tract, the optic and the acoustic radiations were used to begin the relevant delineations.

The corpus callosum was mapped starting from the brain midline and following the fibers laterally until they could no longer be distinguished at high magnification (up to 400×). The identification of the long-association tracts, such as the superior longitudinal fascicle, began in the middle compact part of the tract (Fig. 2). Fibers were followed towards the periphery in the anterior–posterior direction for as long as they could be differentiated from the background tissue.

In a next step, the fibers were interactively marked in each digitized histological image using an image analyzer (KS400© V2.0, Kontron, Germany), and 3-D reconstructed (Figs. 1c, 2b). The labeling procedure was validated by two independent observers: the intra- and inter-rater variability did not exceed ±1 mm for each direction (Bürgel et al., 1999). The topographical relationships between the fiber tracts and nuclei as well as the surrounding anatomical landmarks and basal ganglia were observed by simultaneously displaying all structures of the reconstructed data set in a single brain (Figs. 4–6). Visualization was performed in all three orthogonal planes.

The delineated fiber tracts and nuclei were then registered to the anatomic MNI space. "Probability" or "population" maps quantified the relative frequency with which a certain fiber tract or nucleus of the ten brains was present in each voxel of the reference brain. For example, a 50% value of a fiber tract in a certain voxel of the reference brain indicates that the fiber tract was present in that voxel in five out of ten brains. The percentage of overlap was color-coded in steps of 10% (Figs. 7–16). The probabilistic maps serve as a measure of intersubject variability for each voxel of the reference space.

Results

Positions and topographical relationships of fiber tracts and nuclei

We mapped that part of the corticospinal tract, which originates from Brodmann's area 4 (Brodmann, 1909), i.e., from areas 4a and 4p (Geyer et al., 1996). The tract runs through the posterior limb of the internal capsule (Dejerine, 1901; Penfield and Boldrey, 1937; Fries et al., 1993) and reaches the brain stem (Figs. 4a–d, 5a–f, 6a–f).

Two long-association pathways are in close topographical relationship to the corticospinal tract; the superior longitudinal

Table 2
Characterization of fiber tracts

Fiber tract	Connecting	With
Corticospinal tract	Primary motor cortex (area 4)	Spinal cord/motoneurons
Optic radiation	Lateral geniculate body	Primary visual cortex (area 17)
Acoustic radiation	Medial geniculate body	Primary acoustic cortex (area 41/42)
Fornix	Hippocampus	Mamillary body
Cingulum	Anterior thalamus	Hippocampus
Corpus callosum	Connecting right and left hemispheres	
Superior longitudinal fascicle	Frontal lobe (e.g., Broca' region)	Occipital (visual cortex), parietal and temporal (Wernicke's region) cortices
Superior occipito-frontal fascicle	Prefrontal cortex	Limbic/paralimbic areas
Inferior occipito-frontal fascicle	Frontobasal cortex	Parietal cortex
Uncinate fascicle	Orbital cortices	Entorhinal cortex/hippocampal formation

fascicle and superior occipito-frontal fascicle. The lower part of the superior longitudinal fascicle runs lateral to the corticospinal tract, dorsolateral to the putamen and medial to the upper insula (Figs. 4b–d). Lateral to the entrance of the internal capsule, it turns medial and crosses the motor fibers (Figs. 4b+c, 5a+b, 6c–e). It is thought (Dejerine, 1901) that it connects parts of the frontal lobe (Broca's area) with the occipital (visual areas), parietal and temporal lobes (Wernicke's area). Where the tracing became ambiguous (in the most rostral and most caudal sections), we stopped tracking the fibers.

The superior occipito-frontal fascicle forms the medial border of the corticospinal tract and separates it from the lateral ventricles (Figs. 4c, 5b). The fibers run in parallel to the dorsolateral margin of the lateral ventricles below the corpus callosum. It is assumed that the prefrontal cortex projects via the superior occipito-frontal fascicle to limbic and paralimbic association cortices (Nieuwenhuys et al., 1988).

Fibers of the optic radiation take their origin in the lateral geniculate body. This nucleus is part of the metathalamus and has a characteristic laminar pattern. It is located latero-ventrally to the pulvinar (Figs. 4c, 5e, 6c+d). The efferent optic fibers leave the nucleus in a rostro-lateral direction (Figs. 4c, 5e) and form the so-called knee of the optic radiation. More distally, the fibers run in a rostro-dorsal direction around the temporal horn of the lateral ventricle. The optic radiation is ventral to the acoustic radiation (Figs. 4c, 6b) and turns toward the occipital pole in an almost sagittal plane, running laterally to the occipital horn of the lateral ventricle (Figs. 4d–e, 5c–e). The optic fibers surround the occipital horn of the lateral ventricle and the major forceps of the corpus callosum (Figs. 4f, 5c, 6d+e) to cross towards the mesial surface of the brain. They reach their major target at the superior and inferior banks of the calcarine sulcus; Brodmann's area 17 (Amunts et al., 2000) (Figs. 4f, 5c–f, 6a).

The medial geniculate body, another part of the metathalamus, is medial and slightly ventral to the lateral geniculate body. The acoustic radiation leaves the medial geniculate body in a rostro-lateral direction (Figs. 4c, 5e, 6b). It then runs rostro-dorsally to the optic radiation, crosses the temporal isthmus and ascends towards the primary acoustic cortex, i.e., Brodmann's area 41 of Heschl's gyrus (Figs. 4c, 5c–d, 6a–b). As demonstrated in Fig. 3e, for example, the acoustic radiation of the left hemisphere forms an "S"-shaped course when leaving the medial geniculate body and runs through the temporal stem. Below Heschl's gyrus, the fibers change direction at a very sharp angle of about 60°.

Two association pathways, the inferior occipito-frontal and uncinate fascicles, have a close relationship to the optic and acoustic fiber tracts. The inferior occipito-frontal fascicle runs through the temporal isthmus, where it is located in the notch between the acoustic and optic radiations. The latter is also known as Meyer's loop (Glaser, 1978) (Figs. 4c, 6a+b). Laterally, the inferior occipito-frontal fascicle accompanies the uncinate fasciculus. It ascends to the frontobasal white matter at the level of the temporal horn of the lateral ventricle (Figs. 4a, 5d–f, 6b). Medially, the uncinate fascicle approaches the inferior occipito-frontal fascicle and runs through the temporal isthmus from the frontal lobe to the mesial temporal lobe (Figs. 4a, 5e+f, 6b+c). The uncinate fascicle is near the optic radiation at the turning point of the latter (Meyer's loop).

The main efferent system of the hippocampus is the fornix. It starts as a thin layer of fibers on the surface of the hippocampus ("fimbria", Figs. 4c, 6e). The fibers leave the hippocampus at the level of the splenium of the corpus callosum. The fornices of both hemispheres run in a rostro-medial direction along the roof of the lateral ventricle (crura of the fornix; Figs. 4c–d). The left and the right fornices abut each other in the midline (body of fornix; Figs. 4a+b). Rostral to the intraventricular foramen, the fibers descend (column of fornix) and then run caudally to the mamillary bodies (Figs. 4b, 5f). The mamillary bodies project via the mamillo-thalamic tract to the anterior nucleus of the thalamus.

In turn, the anterior thalamic neurons project to the cingulate cortex, especially the posterior ones, and to the hippocampus. Those fibers travel in the cingulum. The cingulum, which is located interior to the cingulate gyrus, forms a compact pathway running in a fronto-occipital direction. In addition to efferents from the anterior thalamic nucleus, the cingulum contains both long and short association fibers, which connect the prefrontal lobes with posterior cortices, including the hippocampal formation. The cingulum bends around the splenium (isthmus of cingulate gyrus; Figs. 4a–e, 5a, 6a) and turns ventro-rostrally into the white matter of the medial occipito-temporal gyrus (Armstrong, 1990).

The stereotaxic coordinates of the fiber tracts and nuclei were determined in all brains and hemispheres. The maximal extent of the fiber tracts and nuclei was defined in the coronal, sagittal and horizontal planes of the standard reference space for all ten brains (Figs. 4–6, Table 3).

Data concerning the stereotaxic location of tracts and regions were compared to those in the Talairach (Talairach and Tournoux, 1988) atlas (Table 4). The present data, however, go beyond the information provided in this atlas by adding information about right-hemispheric fibers and nuclei. The optic and the acoustic radiations have bilaterally asymmetric rostral extents, which differ by up to 1 cm. The spatial extent of fibers and nuclei had larger ranges than found in the corresponding Talairach data. The left corticospinal tract, for example, reaches from horizontal (z) coordinates 88 to −21, whereas the Talairach atlas gives the most ventral level at $z = 16$. The same is true for nuclei. The location of the lateral geniculate body in the x coordinate, for example, may vary by several millimeters.

Intersubject variability in location and extent

The size, stereotaxic location and shape of the fiber tracts varied considerably among the ten brains (Fig. 3). Therefore, we calculated probability maps for the fiber tracts and their related nuclei (Figs. 7–16). The course, extent and variability of each structure were demonstrated in numerous sections of the three orthogonal planes. In the following paragraphs, we describe probability maps, which illustrate the variability in selected sectioning planes. Complete volumetric data of fiber tracts and nuclei can be obtained at http://www.fz-juelich.de/ime.

Corticospinal tract

Figs. 8a–u demonstrate the spatial variability of the corticospinal tract analyzed in the present study. Two interesting aspects were observed: (i) the degree of intersubject variability shifts along its course, with the highest variability found immediately below the primary motor cortex (e.g., Fig. 7d). The variability decreases (more overlap among the ten brains) in the corona radiata close to the internal capsule. The lowest variability (highest overlap) was found within the internal capsule. Below the internal capsule, the variability of the corticospinal tract

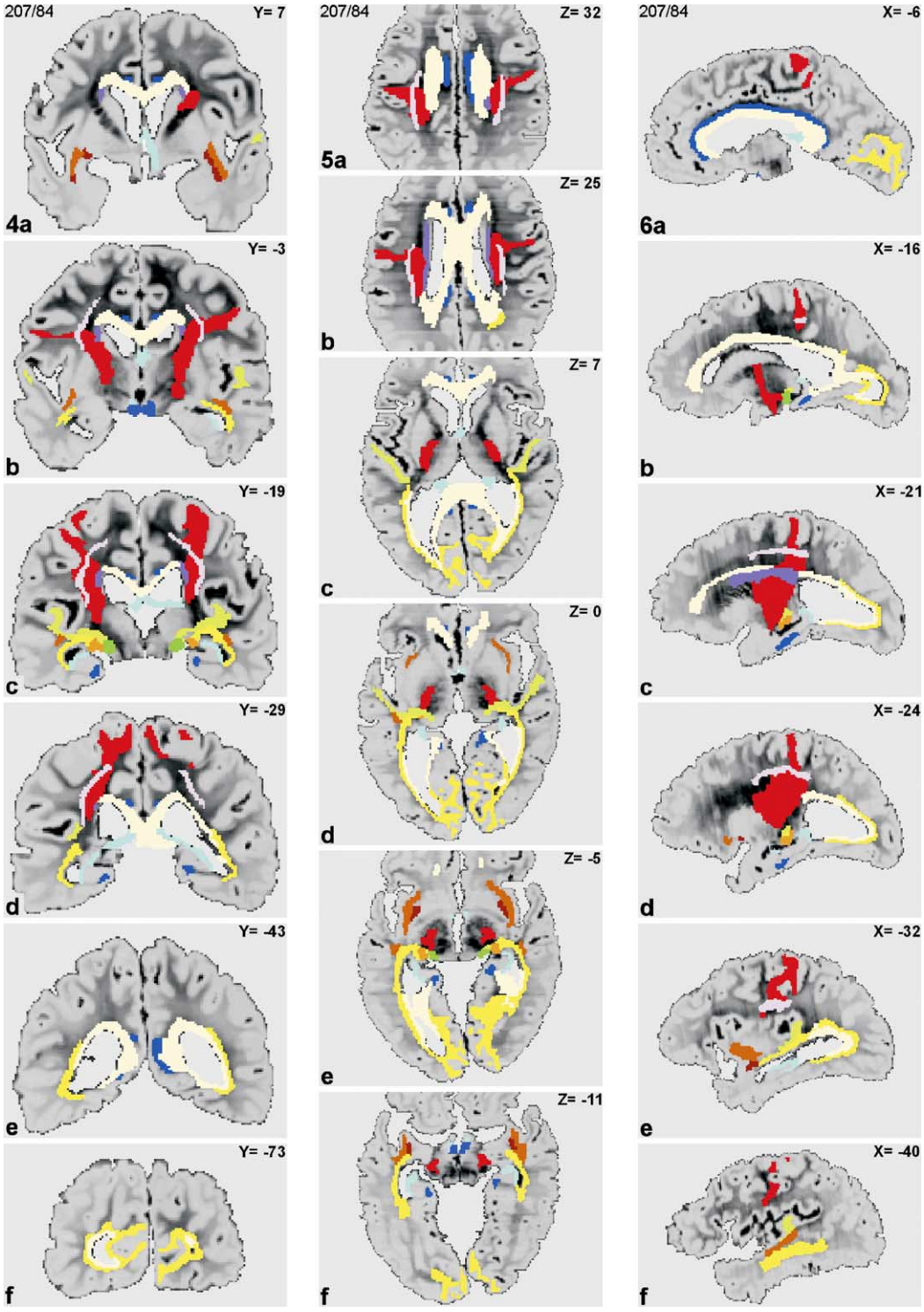

Fig. 4. Coronal sections of brain 207/84 after affine, linear transformation to anatomical MNI space (orientation according to AC–PC plane) at different fronto-occipital levels. Here and below—x is the distance in millimeters to the right (+) or to the left (−) of the midsagittal line; y is the distance anterior (+) or posterior (−) to the vertical plane through the anterior commissure; z is the distance above (+) or below (−) the intercommissural line (AC–PC line). All 13 fiber tracts and nuclei were color-coded and superimposed (color coding is provided at the bottom of Figs. 1–3).

Fig. 5. Horizontal sections of brain 207/84 at different dorso-ventral levels from $z = 32$ to $z = -11$. Designations as above.

Fig. 6. Sagittal sections of brain 207/84 of the left hemisphere from $x = -6$ to $x = -40$. Designations as above.

Table 3
Extent of the left- and right-hemispheric (left, right) parts of the fiber tracts and delineated nuclei (N = 10)

Fiber tracts and nuclei	x				y				z			
	Left		Right		Left		Right		Left		Right	
	From	To	From	To	From	To	From	To	From	To	From	To
Corticospinal tract	−59	0	1	64	5	−53	2	−52	−21	88	−21	89
Optic radiation	−48	1	2	50	−3	−111	−3	−111	−27	40	−22	42
Lateral geniculate body	−29	−15	18	31	−18	−35	−18	−33	−14	7	−12	4
Acoustic radiation	−61	−14	15	64	6	−42	7	−38	−11	27	−12	23
Medial geniculate body	−20	−9	10	23	−23	−35	−19	−34	−13	5	−14	4
Fornix	−37	0	1	43	3	−46	4	−45	−17	31	−15	31
Mamillary body	−6	0	1	10	−1	−18	−1	−18	−15	−4	−16	−4
Cingulum	−27	0	1	31	40	−59	37	−58	−28	44	−27	47
Corpus callosum	−44	–	–	46	43	−94	43	−92	−14	46	−11	47
Sup. long. fasc.	−37	−17	15	39	3	−50	−6	−49	0	60	0	65
Sup. occ.-frontal fasc.	−28	−15	17	29	32	−39	32	−40	1	42	1	48
Inf. occ.-frontal fasc.	−47	−20	19	47	18	−34	22	−33	−17	12	−16	13
Uncinate fascicle	−39	−16	23	41	14	−14	14	−14	−23	4	−23	5

Coordinates are in anatomical MNI space (orientation according the AC–PC line) and refer to the maximal extents of the whole sample of ten brains in each direction. x is the distance in millimeters to the right (+) or to the left (−) of the midsagittal line; y is the distance anterior (+) or posterior (−) to the vertical plane through the anterior commissure; z is the distance above (+) or below (−) the intercommissural line (AC–PC line). The corpus callosum and the fornix cross the midline of the brain and, therefore, were only defined by their most lateral x coordinates (i.e., from the most left position to the most right one). The optic radiation is located close to the midline. Its left-hemispheric portion reaches slightly into the right stereotaxic space. Such a shift has already been shown for area 17 (i.e., the target of the optic radiation; Amunts et al., 2000) and is related to macroscopical asymmetry of the brain shape. Sup. long. fasc.—superior longitudinal fascicle; Sup. occ.-frontal fasc.—superior occipito-frontal fascicle; Inf. occ.-frontal fasc.—inferior occipito-frontal fascicle.

increased again, reaching an overlap of about 60–80% just before entering the brainstem. (ii) The intersubject variability of the corticospinal tract differed between the hemispheres. This tract was less variable in the left than in the right hemisphere. No differences in variability were found in this or the following tracts with respect to gender.

Optic radiation

The optic radiation (Figs. 8a–u) was more variable than the corticospinal tract. Variability was low near the lateral geniculate body, i.e., in the isthmus of the temporal lobe (Figs. 8l+m) and in the posterior part of the tract. The lateral geniculate body showed a very low variability in location. A 100% overlap of the lateral geniculate bodies of the ten brains was found in some voxels in the right hemisphere, but not in the left. Thus, an interhemispheric difference in the degree of variability was observed. In contrast to the corticospinal tract, the optic radiation was less variable in the right than left hemisphere.

Table 4
Extent of the left-hemispheric parts of fiber tracts and nuclei according to the atlas system of Talairach and Tournoux (1988)

Fiber tracts and nuclei	x		y		z	
Corticospinal tract	−51	−3	−35	0	16	65
Optic radiation	−37	−21	−100	−24	−8	12
Lateral geniculate body	−21	−21	−24	−24	−1	−1
Acoustic radiation	–	–	−32	−20	–	–
Medial geniculate body	−17	−13	−24	−24	−4	−1
Fornix	−21	−3	−35	0	−8	12
Mamillary body	−3	−3	−12	−8	−8	−8
Cingulum	−17	−9	−40	32	−12	32
Corpus callosum	−13	0	−40	32	−1	28
Sup. long. fasc.	−37	−33	−32	24	12	28
Occ.-frontal fasc.	−25	−17	−35	28	1	32
Uncinate fascicle	−33	−25	4	20	−12	−12

Designation as in Table 3 above.

Acoustic radiation

The acoustic radiation (Figs. 10a–c) showed a higher degree of variability than the optic radiation. At the origin of the acoustic radiation from the rostro-lateral part of the medial geniculate body, the overlap was only about 30–50%. While ascending into the white matter of the transverse gyrus of Heschl, the variability decreased, and a maximal overlap of 90% was reached. The location of the medial geniculate body also varied considerably between the brains. A maximum overlap of only 70% was found. A clear interhemispheric difference was not seen.

Fornix and cingulum

The fibers of the fornix (Figs. 11a–c) showed an overlap of 70–90% (maximal overlap of 100% in a few voxels) ventral to the splenium of the corpus callosum. In contrast, maximal variability (overlap 30–50%) was found both in the fimbria and the columns of the fornix. The mamillary bodies revealed a moderate variability (overlap 60–80%). The cingulum (Figs. 12a–c) showed an even higher variability in the precallosal region (approximately 30–50% overlap). While running through the isthmus of the cingulate gyrus and towards the parahippocampal gyrus, the overlap increased up to 100%.

Commissural and association pathways

The highest overlap of individual fibers was found in the corpus callosum (Figs. 9a–u). Extended regions with a 100% overlap were located in the splenium, the trunk and the genu. The variability of the corpus callosum increased slightly in the splenium as compared to the trunk and the genu.

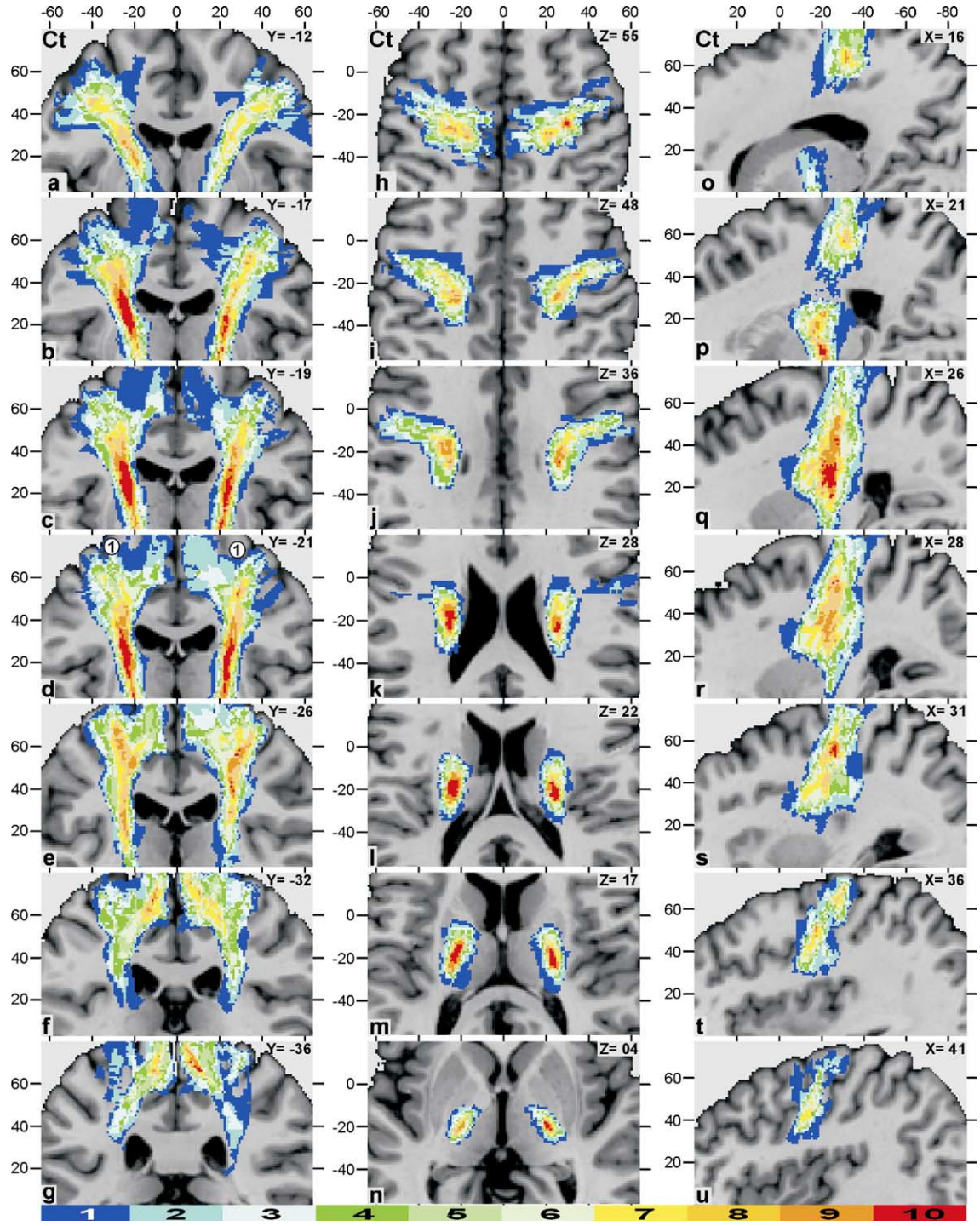

Fig. 7. Probabilistic maps of the corticospinal tract (Ct) in different coronal (a–g), horizontal (h–n) and sagittal (o–u) sections in anatomical MNI reference space. The color bars indicate the absolute frequency of voxels containing the corticospinal tract from 1 (dark blue) to 10 (red, overlap of all ten brains) individual brains. For example, yellow means that 8 of 10 tracts overlapped in this particular voxel. Designations as above.

Long-association fiber tracts

The superior longitudinal fascicle connects mainly occipital (Brodmann's areas 18 and 19) with lateral frontal association cortices (Figs. 13a–c) and has a considerably lower overlap (approximately 40–60%) than the corpus callosum. Maximal overlap (100% in a few voxels) was found in a small region between the insula and the corticospinal fibers.

The variability of the superior occipito-frontal fascicle (Figs. 14a–c) was high. This was particularly true for its occipital part, which is located medial to the corticospinal fibers. A slightly higher degree of overlap was found more frontally, at the transition of the caput to the corpus of the caudate nucleus. The inferior occipito-frontal fascicle runs through the isthmus of the temporal lobe medial to the lower insula (Figs. 15a–c), where it showed an overlap of 70–90%. The fibers spread out from there in frontal and

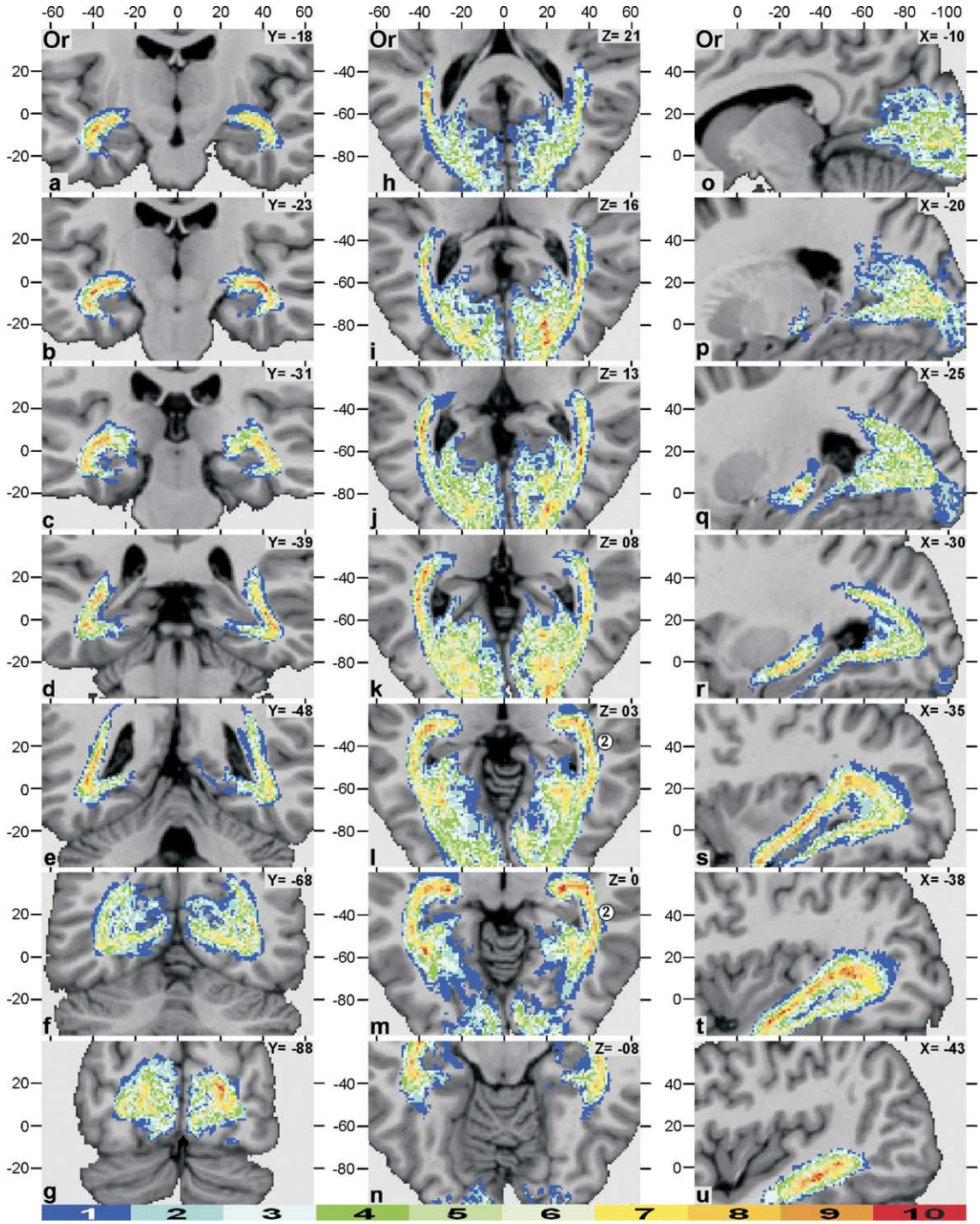

Fig. 8. Probabilistic maps of the optic radiation (Or) in different coronal (a–g), horizontal (h–n) and sagittal (o–u) sections of the reference brain. Designations as above.

occipital directions, and the variability increased (overlap of approximately 30–50%). Finally, the uncinate fascicle (Figs. 16a–c) overlapped at a level of approximately 40–70%.

Discussion

The aim of the present study was to provide stereotaxic maps of important fiber tracts and associated nuclei based on their microscopic appearance in histological myelin-stained sections. The application of a modified Heidenhain–Woelcke staining method, developed to identify fiber tracts in histological sections of adult human brains by our group (Bürgel et al., 1999), enabled us to map them. The fibers were warped to the anatomical MNI reference space, a widely used reference space for functional and anatomical MR studies. The individual variability in 3-D topography and size of fiber tracts and nuclei was quantified by calculating probability maps of fiber tracts and nuclei. This

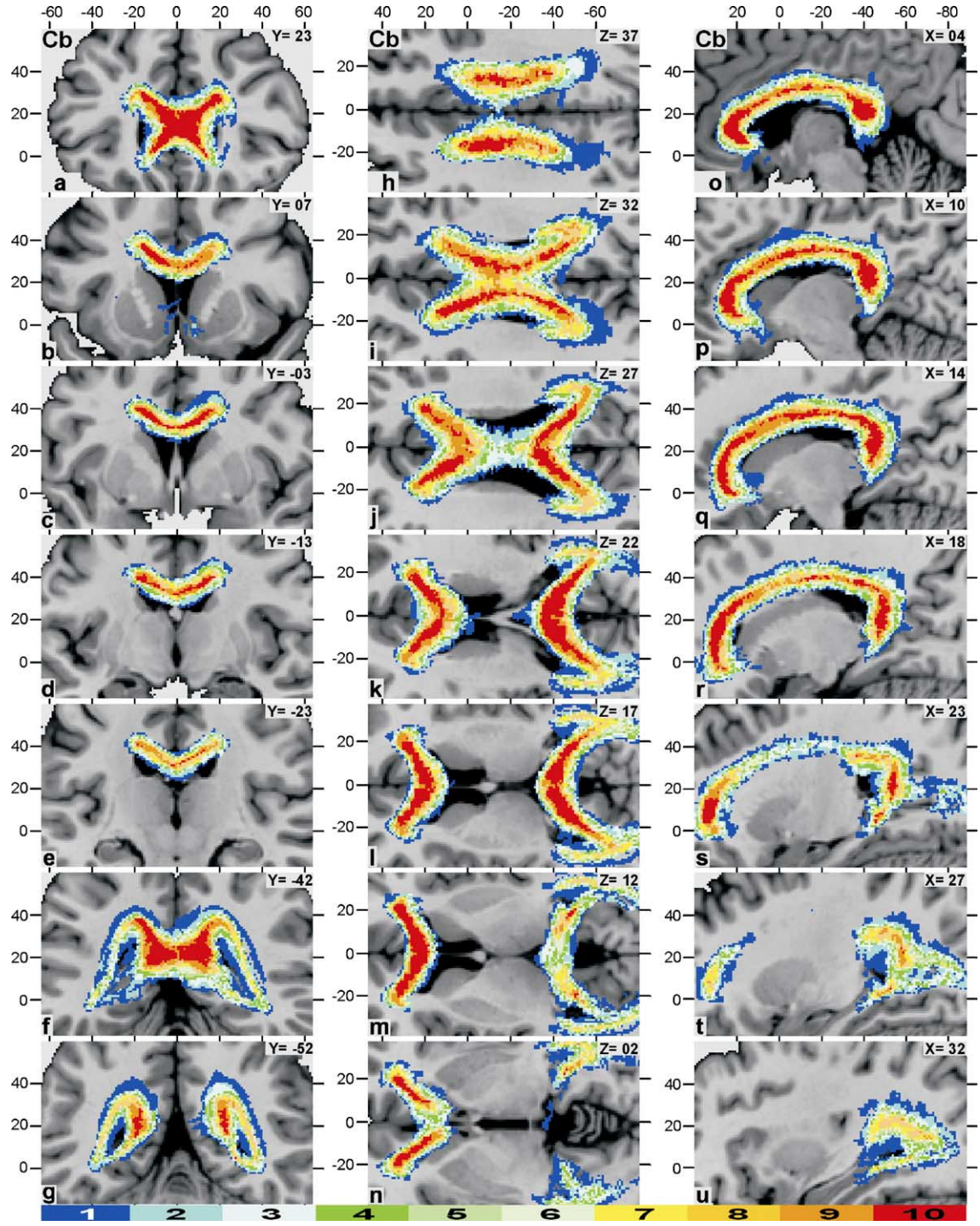

Fig. 9. Probabilistic maps of the callosal body (Cb) in different coronal (a–g), horizontal (h–n) and sagittal (o–u) sections of the reference brain. Designations as above.

stereotaxic information is superior to that of the Talairach atlas (Talairach and Tournoux, 1988) in several respects—(i) it is based on a microscopic delineation, and (ii) it shows and quantifies interhemispheric and intersubject differences in the extent and location of fibers and nuclei.

The microscopic mapping may result in a more precise delineation of fiber tracts and enables mapping in some portions of fiber tracts that are beyond the resolution of alternative mapping tools, e.g., MRI, DT-MRI. Better spatial resolution is particularly helpful in regions where fibers spread out, as when the fibers of the corpus callosum approach the cortical ribbon or when fibers come into close contact with neighboring fiber tracts. The latter situation was found, for example, where the corticospinal tract runs through the brain stem. With our method, we were able to follow the cortico-spinal tract to $z = -21$.

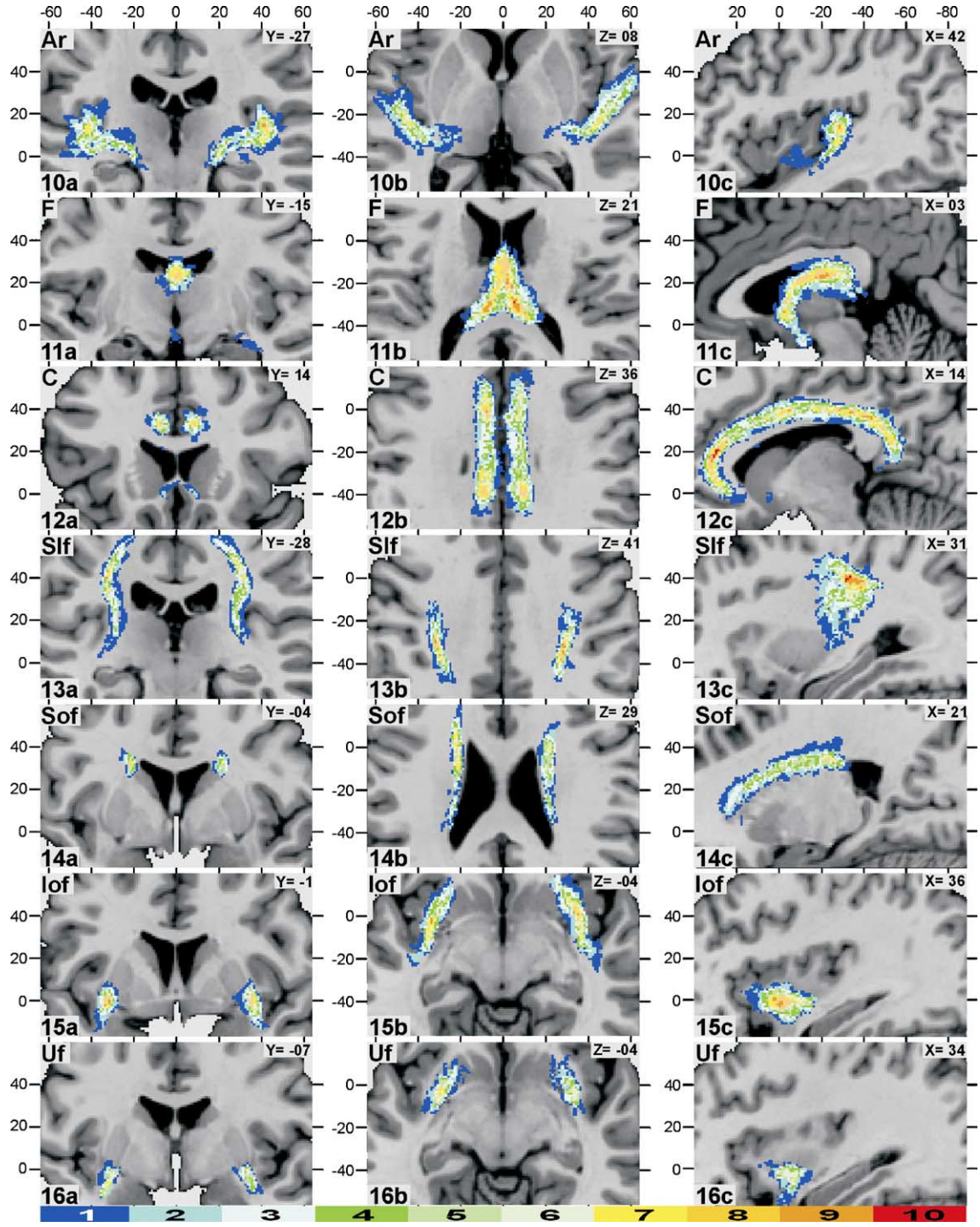

Fig. 10–16. Probabilistic maps of the acoustic radiation (Ar), fornix (F), cingulum (C), superior longitudinal fascicle (Slf), superior occipito-frontal fascicle (Sof), inferior occipito-frontal fascicle (Iof) and uncinate fascicle (Uf) in coronal (a), horizontal (b) and sagittal (c) sections of the reference brain. Designations as above.

High spatial resolution and thin slices are also required in the region of the temporal isthmus where the acoustic radiation forms an "S"-shaped curve as it runs towards Heschl's gyrus and where other major fiber tracts having multiple fiber directions run within a few millimeters of the acoustic fibers. Without high resolution, the abrupt changes in fiber direction cannot be detected. Resolution limits of current DT-MRI may also interfere with the detection of minor nuclei, which have a diameter of only a few millimeters and poor contrast (e.g., the medial geniculate body). These regions were not problematic in our myelo- and cytoarchitectonic studies.

The quality and precision of the maps of some fiber tracts were improved by defining the starting and end points according to microscopically defined cortical areas. We used such information for the corticospinal tract, the optic and acoustic radiations. These

tracts have a high degree of overlap. Source and end points were missing for long-association fiber tracts, where the precise anatomy of the interconnected areas is less well known. This lack of precision may lead to an underestimation of association fiber tract lengths.

The present maps showed that the delineated fiber tracts and nuclei varied considerably between the brains. In our data, different sources of variability include: (i) brain shape and size, (ii) position and course of the fiber tracts, as well as their origins and targets (e.g., cytoarchitectonic areas, subcortical nuclei) and (iii) methodologies. Gross anatomical variability (i) is the major source of variability (Ono et al., 1990); it ranges from several millimeters to centimeters but is largely eliminated by registration procedures. Cortical folding, especially during development, may produce fiber tract variability (Yakovlev and Lecours, 1967; McArdle et al., 1987; Barkovich et al., 1988; Pujol et al., 1993, 2004; Giedd et al., 1999; Paus et al., 2001, Mangin et al., 2004). A second source is microstructural variability (ii) in cortical and subcortical areas that remains after registration (Geyer et al., 1996; Amunts et al., 2000; Rademacher et al., 2002) and therefore influences the variability of the fiber tracts starting from or targeting these areas. This kind of variability is quantified by the probability maps. In addition to this biological variability, certain methods, in particular the non-linear elastic registration (iii), adds some variability. As this is minor, we focus on the second source of variability.

A high degree of overlap, and thus a low intersubject variability, was found in the corticospinal tract and the corpus callosum. To a lesser extent, this was also true in the optic tract. The corticospinal tract and the optic radiation start to myelinate early during ontogeny, the former in the 9th fetal month and the latter around birth (Yakovlev and Lecours, 1967). MR studies of the developing human brain have shown that the internal capsule, the optic radiation and the corpus callosum are among the first to myelinate (for an overview, see Paus et al., 2001). In contrast, long-association fibers, e.g., the superior longitudinal fascicle, and the superior and inferior occipito-frontal fascicles myelinate relatively late (Yakovlev and Lecours, 1967). These fiber tracts have less overlap and more individual variability. It might therefore be speculated that the earlier the fiber tracts are established, the lower the variability.

The acoustic radiation does not fit into this scheme, however. It starts myelinating at the same time as the optic radiation (approximately 3 months postnatal) but shows more variability than the latter. The acoustic and the optic radiations, however, differ with respect to the end points of myelination: this occurs at approximately 4 months for the optic radiation, but at 4 years for the acoustic radiation. This suggests that both the beginning of myelination and its time course influence localization variability. The postnatal ending of myelination also suggests that individual experiences, for example, the languages that the infant is exposed to, might influence variability of acoustic connections more than visual ones.

Our data show that a fiber tract with a lot of variability may be located in close proximity to a tract having low variability. The superior occipito-frontal fascicle, for example, varied considerably in its occipital part, even though that part is located close to corticospinal fibers, which have lower variability. Thus, variability is associated both with a tract's stereotaxic location and its nature.

It is interesting to note that variability was particularly low in regions where the density of fibers was extremely high, as observed in the internal capsule, close to the lateral geniculate body, at the isthmus of the temporal lobe and in the most central parts of the corpus callosum and fornix. These regions are of particular importance with respect to the functional deficits after brain lesions as even small lesions within these regions may cause severe functional deficits.

In conclusion: (i) the stereotaxic maps of ten fiber tracts and three associated nuclei enable a probability-based identification of fiber tracts, invisible in routine, T_1-weighted MRIs of the living human brain, (ii) the intersubject variability of the fiber tracts and nuclei differs according to the fiber tract and its particular location, (iii) the stereotaxic coordinates, which are provided by the Talairach (Talairach and Tournoux, 1988) atlas, underestimate the extent and size of the fiber tracts and nuclei and do not represent a reliable and precise anatomical reference of fiber tracts and (iv) comparing microstructurally defined fiber tracts with data obtained in DT-MRI and tractography (as published recently by Mori et al., 2005; Wakana et al., 2004) permits researchers to evaluate in vivo fiber tracking in detail.

Acknowledgments

This Human Brain Project/Neuroinformatics research is funded by the National Institute of Biomedical Imaging and Bioengineering, the National Institute of Neurological Disorders and Stroke and the National Institute of Mental Health. We are grateful to Este Armstrong for helpful comments and discussion.

References

Amunts, K., Zilles, K., in press. Atlases of the human brain: tools for functional neuroimaging. In: Zaborski, L., Wouterlood, F., Lanciego, J.L. (Eds.), *Neuroanatomical Tract Tracing 3: Molecules–Neurons–Systems*. Springer, Berlin, Germany.

Amunts, K., Malikovic, A., Mohlberg, H., Schormann, T., Zilles, K., 2000. Brodmann's areas 17 and 18 brought into stereotaxic space—Where and how variable? NeuroImage 11, 66–84.

Amunts, K., Weiss, P.H., Mohlberg, H., Pieperhoff, P., Gurd, J., Shah, J.N., Marshall, C.J., Fink, G.R., Zilles, K., 2004. Analysis of the neural mechanisms underlying verbal fluency in cytoarchitectonically defined stereotaxic space—The role of Brodmann's areas 44 and 45. NeuroImage 22 (1), 42–56.

Ardekani, B.A., Nierenberg, J., Hoptman, N.J., Javitt, D.C., Lim, K.O., 2003. MRI study of white matter diffusion anisotropy in schizophrenia. NeuroReport 14, 2025–2029.

Armstrong, E., 1990. Limbic thalamus. In: Paxinos, G. (Ed.), The Human Nervous System. Academic Press, San Diego, pp. 469–481.

Axer, H., Keyserlingk, D.G., 2000. Mapping of fibre orientation in human internal capsule by means of polarized light and confocal scanning laser microscopy. J. Neurosci. Methods 94, 165–175.

Barker, G.J., 2001. Diffusion-weighted imaging of the spinal cord and optic nerve. J. Neurol. Sci. 186, S45–S49.

Barkovich, A.J., Kjos, B.O., Jackson Jr., D.E., Norman, D., 1988. Normal maturation of the neonatal and infant brain: MR imaging at 1.5 T. Radiology 166, 173–180.

Basser, P.J., Jones, D.K., 2002. Diffusion-tensor MRI: theory, experimental design and data analysis—A technical review. NMR Biomed. 15, 456–467.

Basser, P.J., Pierpaoli, C., 1994. Estimation of the effective self-diffusion tensor from the NMR spin echo. J. Magn. Reson., Ser. B 111, 209–219.

Basser, P.J., Pajevic, S., Pierpaoli, C., Duda, J., Aldroubi, A., 2000. In

vivo fibre tractography using DT-MRI data. Magn. Reson. Med. 44, 625–632.
Brodmann, K., 1909. Vergleichende Lokalisationslehre der Grosshirnrinde. Barth, Leipzig.
Büchel, C., Raedler, T., Sommer, M., Sach, M., Weiller, C., Koch, M.A., 2004. White matter asymmetry in the human brain: a diffusion tensor MRI study. Cereb. Cortex 14, 945–951.
Bürgel, U., Mecklenburg, I., Blohm, U., Zilles, K., 1997. Histological visualization of long fibre tracts in the white matter of adult human brains. J. Brain Res. 38, 397–404.
Bürgel, U., Schormann, T., Schleicher, A., Zilles, K., 1999. Mapping of histologically identified long fibre tracts in human cerebral hemispheres to the MRI-volume of a reference brain: position and spatial variability of the optic radiation. NeuroImage 10, 489–499.
Clark, C.A., Barker, G.J., Tofts, P.S., 1999. Magnetic resonance diffusion imaging of the human cervical spinal cord in vivo. Magn. Reson. Med. 41, 1269–1273.
Clarke, S., 1994. Modular organization of human extrastriate visual cortex: evidence from cytochrome oxidase pattern in normal and macular degeneration cases. Eur. J. Neurosci. 6, 725–736.
Clarke, S., Miklossy, J., 1990. Occipital cortex in man: organization of callosal connections, related myelo- and cytoarchitecture, and putative boundaries of functional visual areas. J. Comp. Neurol. 298, 188–214.
Coenen, V.A., Krings, T., Mayfrank, L., Polin, R.S., Reinges, M.H.T., Thron, A., Gilsbach, J.M., 2001. Three-dimensional visualization of the pyramidal tract in a neuronavigation system during brain tumor surgery: first experiences and technical note. Neurosurgery 49 (1), 86–93.
Collins, D.L., Neelin, P., Peters, T.M., Evans, A.C., 1994. Automatic 3D intersubject registration of MR volumetric data in standardized Talairach space. J. Comput. Assist. Tomogr. 18 (2), 192–205.
Conturo, T.E., Lori, N.F., Cull, T.S., Akbudak, E., Snyder, A.Z., Shimony, J.S., McKinstry, R.C., Burton, H., Raichle, M.E., 1999. Tracking neuronal fibre pathways in the living human brain. Proc. Natl. Acad. Sci. 96, 10422–10427.
Dejerine, J., 1901. Anatomie des centres nerveux. Reuff, Paris.
Di Virgilio, G., Clarke, S., 1997. Direct interhemispheric visual input to human speech areas. Hum. Brain Mapp. 5, 347–354.
Evans, A.C., Collins, D.L., Mills, S.R., Brown, E.D., Kelly, R.L., Peters, T.M., 1993. 3D statistical neuroanatomical models from 305 MRI volumes. IEEE/NSS-MI Symp., 1813–1817.
Flechsig, P., 1920. Anatomie des menschlichen Gehirns und Rückenmarks auf myelogenetischer Grundlage. Thieme, Leipzig.
Foong, J., Symms, M.R, Barker, G.J., Maier, M., Miller, D.G.H., Ron, M.A., 2002. Investigating regional white matter in schizophrenia using diffusion tensor imaging. NeuroReport 13, 333–336.
Fries, W., Danek, A.D., Scheidtmann, K., Hamburger, C., 1993. Motor recovery following capsular stroke. Role of descending pathways from multiple motor areas. Brain 108, 697–733.
Geyer, S., Ledberg, A., Schleicher, A., Kinomura, S., Schormann, T., Bürgel, U., Klingberg, T., Larsson, J., Zilles, K., Roland, P.E., 1996. Two different areas within the primary motor cortex of man. Nature 382, 805–807.
Giedd, J.N., Blumenthal, J., Jeffries, N.O., Castellanos, F.X., Liu, H., Zijdenbos, A., Paus, T., Evans, A.C., Rapoport, J.L., 1999. Brain development during childhood and adolescence: a longitudinal MRI study. Nat. Neurosci. 2, 861–863.
Glaser, J.S., 1978. Neuro-ophthalmology. Harper and Row, Hagerstown.
Hagemann, P., Thiran, J.P., Jonasson, L., Vandergheynst, P., Clarke, S., Maeder, P., Meuli, R., 2003. DTI mapping of human brain connectivity: statistical fibre tracking and virtual dissection. NeuroImage 19, 545–554.
Henn, S., Schormann, T., Engler, K., Zilles, K., Witsch, K., 1997. Elastische Anpassung in der digitalen Bildverarbeitung auf mehreren Auflösungsstufen mit Hilfe von Mehrgitterverfahren. In: Paulus, E., Wahl, F.M. (Eds.), Informatik aktuell. Springer, Berlin, Germany, pp. 392–399.
Holmes, C.J., Hoge, R., Collins, L., Woods, R., Toga, A.W., Evans, A.C., 1998. Enhancement of MR images using registration for signal averaging. J. Comput. Assist. Tomogr. 22 (2), 324–333.
Hömke, L., 2005. A multigrid method for anisotrophic PDE's in elastic image registration. Proceedings of the Twelfth Copper Mountain Conference on Multigrid Methods. Copper Mountain, Colorado, USA.
Iwasawa, T., Matoba, H., Ogi, T., Kurihara, H., Saito, K., Yoshida, T., Matsubara, S., Nozaki, A., 1997. Diffusion-weighted imaging of the human optic nerve: a new approach to evaluate optic neuritis in multiple sclerosis. Magn. Reson. Med. 38, 484–491.
Koch, M.A., Glauche, V., Finsterbusch, J., Nolte, U.G., Frahm, J., Weiller, C., Büchel, C., 2002. Distortion-free diffusion tensor imaging of cranial nerves and of inferior temporal and orbitofrontal white matter. NeuroImage 17, 497–506.
Kretschmann, H.-J., Weinrich, W., 1996. Dreidimensionale Computergraphik neurofunktioneller Systeme. Thieme, Stuttgart, Germany.
Krings, T., Coenen, V.A., Axer, H., Möller-Hartmann, W., Mayfrank, L., Weidemann, J., Kränzlein, H., Gilsbach, J.M., Thron, A., 2001. In vivo 3D visualization of pyramidal tracts using anisotropic diffusion weighted magnetic resonance imaging. Neurosci. Lett. 307, 192–196.
Kubicki, M., Park, H., Westin, C.F., Nestor, P.G., Mulkern, R.V., Maier, S.E., Niznikiewicz, M., Connor, E.E., Levitt, J.J., Frumin, M., Kikinis, R., Jolesz, F.A., McCarley, R.W., Shenton, M.E., 2005. DTI and MTR abnormalities in schizophrenia: analysis of white matter integrity. NeuroImage 26 (4), 1109–1118.
Le Bihan, D., Breton, E., Lallarmand, D., Grenier, P., Canabis, E., Laval-Jeatet, M., 1986. MR imaging of intravoxel incoherent motions: applications to diffusion and perfusion in neurological disorders. Radiology 161, 401–407.
Le Bihan, D., Mangin, J.F., Poupon, C., Clark, C.A., Pappata, S., Molko, N., Chabriat, H., 2001. Diffusion tensor imaging: concepts and applications. J. Magn. Reson. Imag. 13, 534–546.
Makris, N., Worth, A.J., Sorensen, A.G., Papadimitriou, G.M., Wu, O., Reese, T.G., Wedeen, V.J., Davis, T.L., Stakes, J.W., Caviness, V.S., Kaplan, E., Rosen, B.R., Pandya, D.N., Kennedy, D.N., 1997. Morphometry of in vivo human white matter association pathways with diffusion-weighted magnetic resonance imaging. Ann. Neurol. 42, 951–962.
Mangin, J.F., Riviere, D., Cachia, A., Duchesnay, E., Cointepas, Y., Papadopoulos-Orfanos, D., Scifo, P., Ochiai, T., Brunelle, F., Regis, J., 2004. A framework to study the cortical folding patterns. NeuroImage 23, S129–S138.
McArdle, C.B., Richardson, C.J., Nicholas, D.A., Amparo, E.G., 1987. Developmental features of the neonatal brain: MR imaging: Part I. Gray–white matter differentiation and myelination. Radiology 162, 223–229.
Merker, B., 1983. Silver staining of cell bodies by means of physical development. J. Neurosci. 9, 235–241.
Miklossy, J., van der Loos, H., 1991. The long-distance effects of brain lesions: visualization of myelinated pathways in the human brain using polarizing and fluorescence microscopy. J. Neuropathol. Exp. Neurol. 50, 1–15.
Mohlberg, H., Lerch, J., Amunts, K., Evans, E., Zilles, K., 2003. Probabilistic cytoarchitectonic maps transferred into MNI space. NeuroImage 19 (2), S1–e1763.
Mori, S., van Zijl, P.C.M., 2002. Fibre tracking: principles and strategies—A technical review. NMR Biomed. 15 (7–8), 468–480.
Mori, S., Wakana, S., van Zijl, P.C.M., Nagae-Poetscher, L.M., 2005. MRI atlas of the human white matter. Elsevier, Amsterdam, The Netherlands.
Mufson, E.J., Brady, D.R., Kordower, J.H., 1990. Tracing neuronal connections in postmortem human hippocampal complex with the carbocyanine dye DiI. Neurobiol. Aging 11, 649–653.
Nieuwenhuys, A., Voogd, J., Van Huijzen, C., 1988. The Human Central Nervous System: a Synopsis and Atlas. Springer, Berlin, Germany.
Ono, M., Kubik, S., Abernathey, C.D., 1990. Atlas of the Cerebral Sulci. Thieme, Stuttgart, Germany.
Parker, G.J.M., Stephan, K.E., Barker, G.J., Rowe, J.B., MacManus, D.G., Wheeler-Kingshot, C.A.M., Ciccarelli, O., Passingham, R.E., Spinks,

R.L., Lemon, R.N., Turner, R., 2002. Initial demonstration of in vivo tracing of axonal projections in the macaque brain and comparison with the human brain using diffusion tensor imaging and fast marching tractography. NeuroImage 15, 797–809.

Paus, T., Collins, D.L., Evans, A.C., Leonard, B., Pike, B., Zijdenbos, A., 2001. Maturation of white matter in the human brain: a review of magnetic resonance studies. Brain Res. Bull. 54, 225–266.

Penfield, W., Boldrey, E., 1937. Somatic motor and sensory representation in the cerebral cortex of man as studied by electrical stimulation. Brain 60, 389–443.

Piearpoli, C., Jezzard, P., Basser, P.J., Barnett, A., Di Chiro, G., 1996. Diffusion tensor MR imaging of the human brain. Radiology 201, 637–648.

Pujol, J., Vendrell, P., Junque, C., Marti-Vilalta, J.L., Capdevila, A., 1993. When does human brain development end? Evidence of corpus callosum growth up to adulthood. Ann. Neurol. 34, 71–75.

Pujol, J., Lopez-Sala, A., Sebastian-Galles, N., Deus, J., Cardoner, N., Soriano-Mas, C., Moreno, A., Sans, A., 2004. Delayed myelination in children with developmental delay detected by volumetric MRI. NeuroImage 22, 897–903.

Rademacher, J., Bürgel, U., Geyer, S., Schormann, T., Schleicher, A., Freund, H.-J., Zilles, K., 2001. Variability and asymmetry in the human precentral motor system—A cytoarchitectonic and myeloarchitectonic brain mapping study. Brain 124, 2232–2258.

Rademacher, J., Bürgel, U., Zilles, K., 2002. Stereotaxic localization, intersubject variability, and interhemispheric differences of the human auditory thalamocortical system. NeuroImage 17, 142–160.

Ramnani, N., Behrens, T.E.J., Penny, W., Matthews, P.M., 2004. New approaches for exploring anatomical and functional connectivity in the human brain. Biol. Psychiatry 56, 613–619.

Roland, P.E., Zilles, K., 1994. Brain atlasses–A new research tool. TINS 17, 458–467.

Schoth, F., Krings, T., 2005. Diffusion-tensor imaging in septo-optic dysplasia. Neuroradiology 46 (9), 759–763.

Schormann, T., Zilles, K., 1998. Three-dimensional linear and nonlinear transformations: an integration of light microscopical and MRI data. Hum. Brain Mapp. 6, 339–347.

Stieltjes, B., Kaufmann, W.E., VanZijl, P.C., Fredericksen, K., Pearlson, G.D., Solaiyappan, M., Mori, S., 2001. Diffusion tensor imaging and axonal tracking in the human brainstem. NeuroImage 14, 723–735.

Talairach, J., Tournoux, P., 1988. Co-planar Stereotaxic Atlas of the Human Brain. Thieme, Stuttgart, Germany.

Turner, R., Le Bihan, D., Maier, J., Vavrek, R., Hedges, L.K., Pekar, J., 1990. Echo-planar imaging of intravoxel incoherent motion. Radiology 177, 407–414.

Virta, A., Barnett, A., Pierpaoli, C., 1999. Visualizing and characterizing white matter fibre structure and architecture in the human pyramidal tract using diffusion tensor MRI. Magn. Res. Imaging 17, 1121–1133.

Wakana, S., Jlang, H., Nagae-Poetscher, L.M., van Zijl, P.C.M., Mori, S., 2004. Fibre tract-based atlas of human white matter anatomy. Radiology 230, 77–87.

Wakana, S., Nagae-Poetscher, L.M., Jlang, H., van Zijl, P.C.M., Golay, X., Mori, S., 2005. Macroscopic orientation component analysis of brain white matter and thalamus based on diffusion tensor imaging. Magn. Res. Med. 53 (3), 649–657.

Werring, D.J., Clark, C.A., Parker, G.J.M., Miller, D.H., Thompson, A.J., Barker, G.J., 1999. A direct demonstration of human visual cortex demonstrated by functional MRI with monocular stimulation. NeuroImage 9, 352–361.

Wiesendanger, E., Clarke, S., Kraftsik, R., Tardif, E., 2004. Topography of cortico-striatal connections in man: anatomical evidence for parallel organization. Eur. J. Neurosci. 20, 1915–1922.

Yakovlev, P.I., Lecours, A.-R., 1967. The myelogenetic cycles of regional maturation of the brain. In: Minkowski, A. (Ed.), Regional Development of the Brain in Early Life. Blackwell, Oxford.

Zilles, K., Schlaug, G., Matelli, M., Luppino, G., Schleicher, A., Qu, M., Dabringhaus, A., Seitz, R., Roland, P.E., 1995. Mapping of human and macaque sensorimotor areas by integrating architectonic, transmitter receptor MRI and PET data. J. Anat. 187, 515–537.

Zilles, K., Dabringhaus, A., Geyer, S., Amunts, K., Qü, M., Schleicher, A., Gilisen, E., Schlaug, G., Steinmetz, H., 1996. Structural asymmetries in the human forebrain and the forebrain of non-human primates and rats. Neurosci. Biobehav. Rev. 20, 593–605.

Zilles, K., Schleicher, A., Langemann, C., Dabringhaus, A., Amunts, K., Morosan, P., Palomero-Gallagher, N., Schormann, T., Mohlberg, H., Bürgel, U., Steinmetz, H., Schlaug, G., Roland, P.E., 1997. Quantitative analysis of sulci in the human cerebral cortex: development, regional heterogeneity, gender difference, asymmetry, intersubject variability and cortical architecture. Hum. Brain Mapp. 5, 218–221.